Available online at www.sciencedirect.com

ScienceDirect

Procedia Engineering 116 (2015) 88 – 96

Procedia Engineering

www.elsevier.com/locate/procedia

8th International Conference on Asian and Pacific Coasts (APAC 2015)

Modelling of Solitary Wave Run-up on an Onshore Coastal Cliff by Smoothed Particle Hydrodynamics Method

Wei Jian[a], Shawn Y. Sim[b,c], Zhenhua Huang[d], Edmond Yat-Man Lo[a,e,*]

[a]*Maritime Institute, Nanyang Technological University, Singapore*
[b]*Asian School of the Environment, Nanyang Technological University, Singapore*
[c]*Earth Observatory of Singapore, Nanyang Technological University, Singapore*
[d]*Department of Ocean and Resources Engineering, School of Ocean and Earth Science and Technology, University of Hawaii at Manoa, USA*
[e]*School of Civil and Environmental Engineering, Nanyang Technological University, Singapore*

Abstract

The solitary wave run-up in the presence of an onshore coastal cliff is investigated using the Smoothed Particle Hydrodynamics (SPH) method. A composite topography made of a steep slope, a gentle beach and a steep coastal cliff was used in the experimental and numerical studies to represent real life scenarios. Comparison with laboratory measurements shows that the SPH model is able to capture the evolution and run-up of solitary waves for both non-breaking and slight breaking cases with reasonable accuracy.

Peer- Review under responsibility of organizing committee , IIT Madras , and International Steering Committee of APAC 2015

Keywords: tsunami run-up; SPH; onshore topography

1. Introduction

It has been widely understood that tsunamis can cause catastrophic damages when it propagates inland. The tsunami waves are capable of destructing offshore and near-shore structures which would then behave as debris flowing inland, claiming lives and obstructing evacuation passages. Understanding the site specific wave characteristics and their interaction with man-made structures are essential for designs of coastal structures. Over the last decades, there have been a number of studies conducted by researchers using experimental and numerical

Peer- Review under responsibility of organizing committee , IIT Madras , and International Steering Committee of APAC 2015
doi:10.1016/j.proeng.2015.08.268

means to understand tsunami wave run-up and its interaction with coastal structures. Thus far, most of these studies have been limited to a gentle sloping plane beach. Complex near-shore interaction between the onshore flows and near-shore topography can play an important role in shaping the site-specific inundation and subsequent interaction with man-made structures. Hill et al. (2012) compared the damage done to the island of Pulau Sibigau with its neighbouring islands by the 2010 earthquake and tsunami event which occurred in the Mentawai Islands off Sumatra, Indonesia. The undulating profile of Pulau Sibigau was significantly influenced by the presence of a very steep inland cliff on site. It is quite common to find this type of steep inland cliffs located closely to shorelines. Such topographical features could result in highly turbulent flows and amplification of flow depth at the vicinity of the cliff. Large scale water sprays and splashing can be generated due to the wave breaking at the cliff.

Solitary waves are often used as initial conditions to approximate tsunami waves because of the hydrodynamic similarity between the two. Numerically predicting solitary wave run-up presents a challenge since it involves nonlinear building of wave front, severe wave breaking and strong turbulent flow. A number of numerical methods have been developed to predict the wave run-up. Most of them are governed by the shallow water equations (SWEs), which works well when the geometry satisfies the long-wave approximation. As the bathymetry and topography profiles become more complex, the numerical results can differ significantly from the measured data. The study on the island Pulau Sibigao by Hill et al. (2012) proved this point after comparing the recorded data with their simulation results. Three-dimensional modelling carried out by Huang et al. (2013) showed that the wave forms under complex near-shore topography can be captured but at the expense of large computational effort. Recent emergence of meshless methods has provided a desirable alternative. Smoothed Particle Hydrodynamics (SPH) method, originally developed for astrophysics (Lucy, 1977; Gingold and Monaghan, 1977), has been under intense development over the last two decades since it was first introduced to model free surface flows (Monaghan, 1992; 1994). Readers are referred to Liu and Liu (2010) for a detailed overview on the SPH methodology. The SPH method was later extended to model solitary wave propagation and impact problems (Monaghan and Kos, 1999). Since then, there have been a large number of published papers reporting on the SPH modelling of wave impact problems. Shao and Lo (2002) and later Shao (2005) studied the solitary wave mechanics, wave interaction with breakwaters and breaking waves. Dalrymple and Rogers (2006) examined the propagation of highly nonlinear and breaking and later reported their modelling of tsunami waves (Rogers and Dalrymple, 2008). Gómez-Gesteira *et al*. (2010) provides an overview on the state-of-art of the SPH and its application in the wave propagation and interaction with coastal structures in both two- and three-dimensional cases.

The objective of this study is to investigate the solitary run-up in the presence of an onshore coastal cliff through laboratory and numerical studies. The so-called DualSPHysics (Crespo et al., 2011; Gomez-Gesteira et al., 2012a, 2012b) numerical model has been used for the scope. The model was developed to run on both CPUs and GPUs which enables large-scale applications to be simulated using the SPH method. Documentations on the validation and implementation of DualSPHysics can be found in Crespo et al. (2011) and Domínguez et al. (2011, 2013a, 2013b). In this paper, the flow depths at various onshore locations under different incident wave levels were simulated using the DualSPHysics model and compared with experimental measurements.

2. Smoothed Particle Hydrodynamics Methodology

2.1. SPH algorithm

The SPH formulations are based on the concept of integral interpolations. By using a kernel function to describe the connectivity between particles, the differential operators in the Navier-Stokes equations can be approximated by summations over discretized particles. For a function F that represents a physical variable over a domain of interest, the concept of integral representation can be written as a convolution product of the function itself and a smooth function called kernel function, $W(r - r', h)$.

$$F(r) = \int F(r')W(r - r', h)dr' \tag{1}$$

where h is the smoothing length that determines the size of the compact support. The kernel function needs to satisfy a number of properties in order to define the interaction between neighbouring particles within a compact support. The quintic kernel proposed by Wendland (1995) has been used in this study for its high order of interpolation at a moderate computational cost.

$$W(r,h)=\alpha_D\left(1-\frac{q}{2}\right)^4(2q+1) \qquad 0\le q\le 2 \tag{2}$$

where q is the non-dimensional distance between particles and $\alpha_D=7/(14\pi h^2)$ for two dimensions and $21/(16\pi h^3)$ for three dimensions.

2.2. Governing equations

The classical SPH formulation assumes the fluid is weakly compressible and solves the hydrodynamic Navier-Stokes equations in the Lagrangian form as follows,

$$\frac{d\rho}{dt}+\rho\nabla\cdot\mathbf{v}=0 \tag{3}$$

$$\frac{d\mathbf{v}}{dt}=-\frac{1}{\rho}\nabla P+\mathbf{g}+\upsilon_0\nabla^2\mathbf{v}+\frac{1}{\rho}\nabla\cdot\vec{\tau} \tag{4}$$

where t is the time, ρ is the density, $\mathbf{v}$ is the flow velocity vector, P is the pressure, υ_0 is the viscosity coefficient, $\mathbf{g}$ is the gravitational acceleration and $\vec{\tau}$ is the SPS stress tensor. To minimize the numerical diffusion arised from the viscosity term, the laminar viscous stresses and sub-particle scale (SPS) turbulence terms are solved in Equation (4). In SPH notations, Equation (4) can be written as (Dalrymple and Rogers, 2006),

$$\frac{d\mathbf{v}_i}{dt}=-\sum_j m_j\left(\frac{P_j}{\rho_j^2}+\frac{P_i}{\rho_i^2}\right)\nabla_i W_{ij}+\mathbf{g}+\sum_j m_j\left(\frac{4\upsilon_0\mathbf{r}_{ij}\cdot\nabla_i W_{ij}}{(\rho_i+\rho_j)(r_{ij}^2+\eta^2)}\right)\mathbf{v}_{ij}+\sum_j m_j\left(\frac{\vec{\tau}_{i,j}^{\,j}}{\rho_j^2}+\frac{\vec{\tau}_{i,j}^{\,i}}{\rho_i^2}\right)\nabla_i W_{ij} \tag{5}$$

where i is the interpolation particle and j denotes all the particles within the region of compact support of the kernel function, defined by h. $\mathbf{r}_{ij}=\mathbf{r}_i-\mathbf{r}_j$, $\mathbf{v}_{ij}=\mathbf{v}_i-\mathbf{v}_j$ and $\eta^2=0.01h^2$.

To close the equations, an equation of state is adopted to relate the pressure with the fluid density, which takes the following form,

$$P=B\left(\left(\frac{\rho}{\rho_0}\right)^\gamma-1\right) \tag{6}$$

where ρ_0 is the reference density set to 1000.0 kg/m^3 for the water, and γ is a constant equal to 7.0. $B=c_0^2\rho_0/\gamma$ sets the maximum limit of density variation allowed in the flow. c_0 is the speed of sound at the reference density, which is set to 50 m/s in this study.

2.3. Wave-maker Theory

Wave generation is normally achieved in SPH by replacing the upstream solid boundary with a wave-maker that moves with a prescribed motion to resemble the real motion took place during the experiments. For the present study, the Rayleigh's solitary wave solution was used to generate the displacement for the piston-type wave-maker.

It has been proved to provide purer and more rapid wave formations with less amplitude loss during propagation when compared with Goring's solution (Katell and Eric, 2002). Assuming small displacements, the paddle position X can be solved explicitly as follows,

$$X(t)=\frac{2H_0}{d\beta}\frac{d\tanh(\beta ct/2)}{d+A\left[1-\tanh^2(\beta ct/2)\right]} \qquad \text{where } \beta=2\sqrt{\frac{3H_0}{4d^2(A+d)}} \text{ and } c=\sqrt{g(H_0+d)} \tag{7}$$

where H_0 is the solitary wave amplitude, d the mean water depth, c the phase speed and β the outskirts decay coefficient.

3. Tsunami wave run-up on a steep coastal cliff

3.1. Experimental set-up

The experimental set-up for this study is shown in Fig. 1. The cross-shore profile is modelled using a composite slope made of three sections, a steep slope of 0.17 m long starting at x = 10.00 m with an angle of 55.7˚, a gentle onshore of ratio 1:15 to resemble the beach and a coastal cliff at the beach section to reproduce real-life topography. The mean water depth, d, is fixed at 0.35 m.

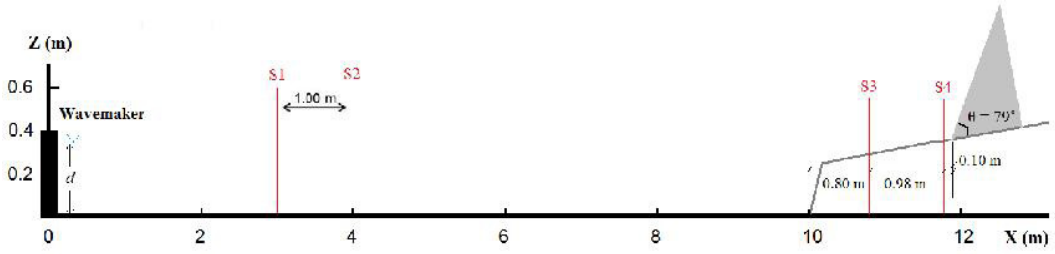

Fig. 1. Experimental set-up.

Solitary waves were generated using a piston wave-maker located at the left boundary of the wave flume. Several incident wave heights and onshore cliff angles were tested in the laboratory. In the present study, results from two incident wave heights, H_0 = 0.025 m and 0.055 m with the largest angle of the cliff θ = 79˚, are investigated and compared with numerical work hereafter.

Acoustic Ultralab sensors were used to record water surface elevations at four cross-shore profiles, namely S1 to S4 as indicated in Fig. 1. In addition to the measurements taken from the sensors, three web cameras were installed to capture the flow patterns. Two cameras were used for the side profile and the other one for plan profile. The videos captured by the cameras were post processed to obtain surface elevations measurements.

3.2. Numerical set-up

The configuration used for SPH simulations were slightly modified from Fig. 1. The distance from the wave-maker to S_1 was reduced from 3.00 m to 0.50 m in the numerical wave flume to reduce computational time. The incident waves generated based on Equation (7) were calibrated against the measurements recorded at S1 to ensure that correct wave characteristics were simulated.

Using this initial configuration, the total number of particles in the numerical work was 110,073 (including 2530 dynamic boundary particles described in Crespo et al. (2007)) based on a uniform particle spacing of 0.005 m. A second-order Symplectic time integration scheme detailed in Gómez-Gesteira et al. (2012) was adopted in the

SPH model with a time step of 1.0×10^{-6} s. The simulation of 10.0 s physical time took 1.96 hours on an NVIDIA Quadro K620 graphics card.

3.3. Results and Discussion

In plane beaches, the waves generally propagate up the beach and reach the run-up limit before moving backwards as a sheet flow. The presence of a cliff alters the onshore flow patterns, making this run-up and drawdown process more complex. As the wave approaches the shoreline, it moves towards the toe of the shoreline cliff as a bore. Upon encountering the cliff, the water mass climbs up along the slope of the cliff causing amplification of the inundation at the toe of the onshore cliff. A steeper cliff angle is expected to result in larger water accumulation in the region and therefore a higher amplification factor. Hereafter, two incident wave heights are investigated and analyzed.

In the case with H_0 = 0.025 m, the solitary wave propagates towards the cliff without prior breaking. Fig. 2 shows the evolution of wave profiles and the corresponding pressure fields as the wave front approaches and climbs up the cliff. At t = 8.0 s, the wave front is seen propagating up the gentle beach section with no sign of breaking. The wave front reaches the toe of the cliff at t = 8.3 s and starts to climb along the slope of the cliff. By t = 8.5 s, a run-up height of approximately 0.06 m can be seen in Fig. 2. The water mass gradually draws back from the cliff after reaching its maximum and flows back to the gentle beach section. The flow depth in the beach section amplifies as the reflected wave propagates past, which is evident in snapshots after t = 9.0 s. The maximum run-up height on the cliff is observed to occur at t = 8.45 s with a distance of approximately 0.015 m up the slope of the cliff.

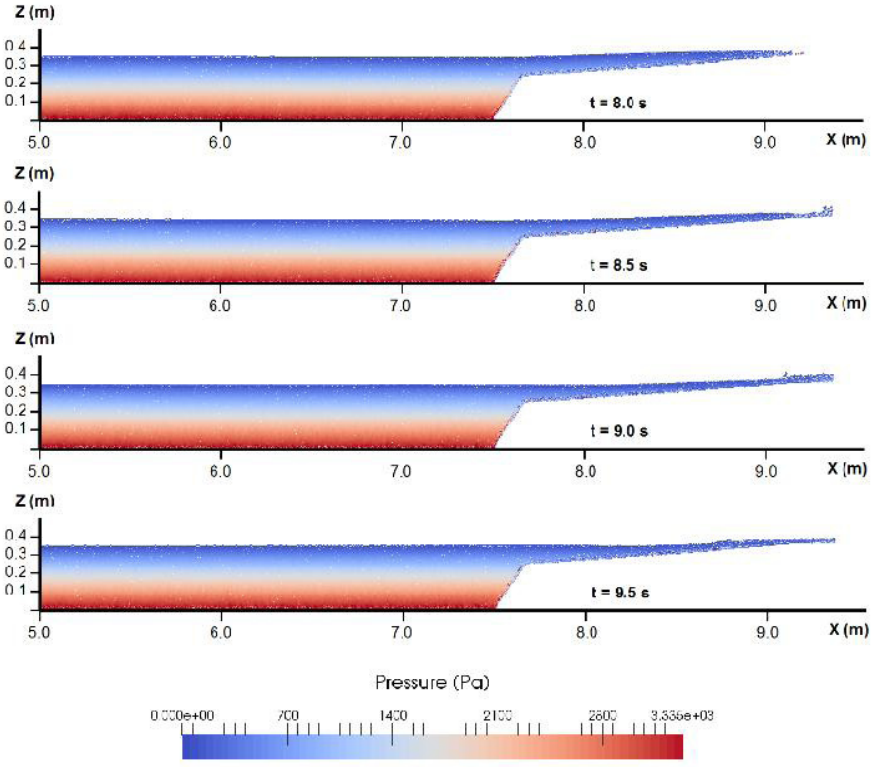

Fig. 2. Solitary wave profiles and pressure fields for H_0 = 0.025 m.

Fig. 3 compares the time history of water levels at S1 to S4 between the SPH results and laboratory measurements. Three particle sizes were used and the corresponding results are shown in Fig.3. It can be seen that the numerical solutions agree well with the experiment data for the propagation and run-up of the solitary wave at all gauges. The slight discrepancy in the slope of the drawback process observed at S3 and S4 is thought to be mainly contributed by the limited amount of particles in the gentle beach region during the retreat of the reflected wave front. It is estimated that the water depth is approximately within the order of 0.02 m during this time, which corresponds to only ten particle spacing at most. Due to the integral interpolation nature of SPH method, these fluid particles are less supported by the limited amount of neighbouring particles available. This could cause particles to move more like a group with an average velocity instead of individual particles. In addition, some pressure disturbances can be observed close to solid boundaries in Fig. 2. These fluctuations in the pressure field can affect the particle movement significantly when the water depth is shallow. It is noted that reducing the particle size can slightly improve on the numerical ability to capture the full extent of the change in water level experienced at S4, but not the discrepancy in the drawback process discussed above.

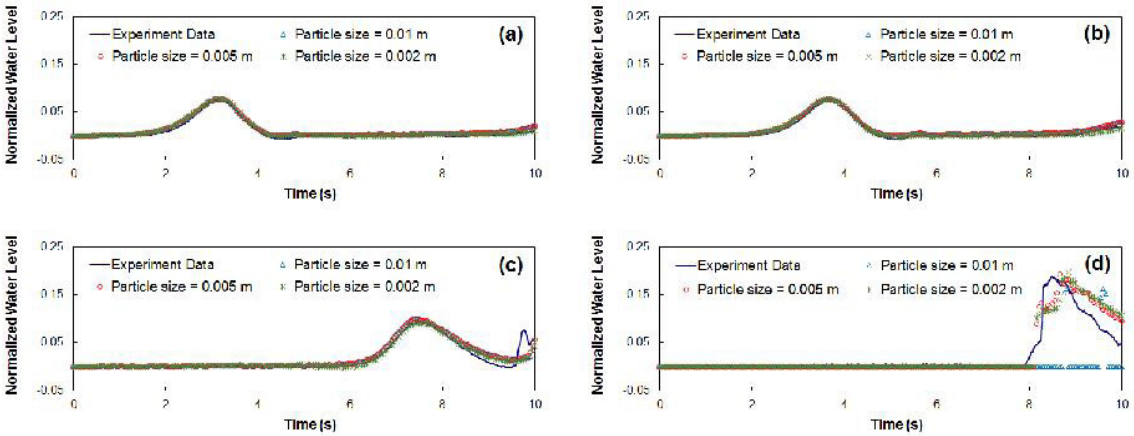

Fig. 3. Time history of water levels at the four monitoring points: (a) S1; (b) S2; (c) S3 and (d) S4 by the SPH model and experimental measurements for $H_0 = 0.025$ m. The normalized water levels are normalized by the mean water depth d.

In the case with $H_0 = 0.055$ m, the incident wave becomes very steep and small-scale breaking took place just prior to the toe of the cliff. Snapshots of the wave profiles at $t = 6.3$ s to 8.0 s simulated by the SPH model are present in Fig. 4. It is clear that the wave front approaching the cliff has a much more pronounced height than the previous case. As the wave propagates further, it breaks and climbs up the cliff until a maximum run-up height is reached at $t = 6.9$ s. This corresponds to a distance of approximately 0.1 m along the slope of the cliff. As the run-up water retreats back from the cliff, it plunges onto the water underneath it as seen in the snapshot at $t = 7.2$ s, causing some water splashes as the two interact. The reflected wave gradually propagates upstream and by $t = 8.0$ s it has established a stable wave form.

Comparisons of time histories of water levels recorded at S1 to S4 from the SPH model and experimental data are shown in Fig. 5. Again, the SPH results have good agreements with the laboratory measurements at S1 to S4. As shown in Fig. 4, the surface elevation at S4 during $t = 6.5$ s and 8.0 s is relatively turbulent due to the small breakings and splashing. This phenomenon was also observed in the experiment and the measurements at S4 taken by the Ultralab sensors and camera images had a discrepancy of 7%. The SPH model is able to capture the maximum water levels observed at S3 and S4, with more accurate drawback velocities after the maxima owing to better kernel support in the beach region with larger incident wave.

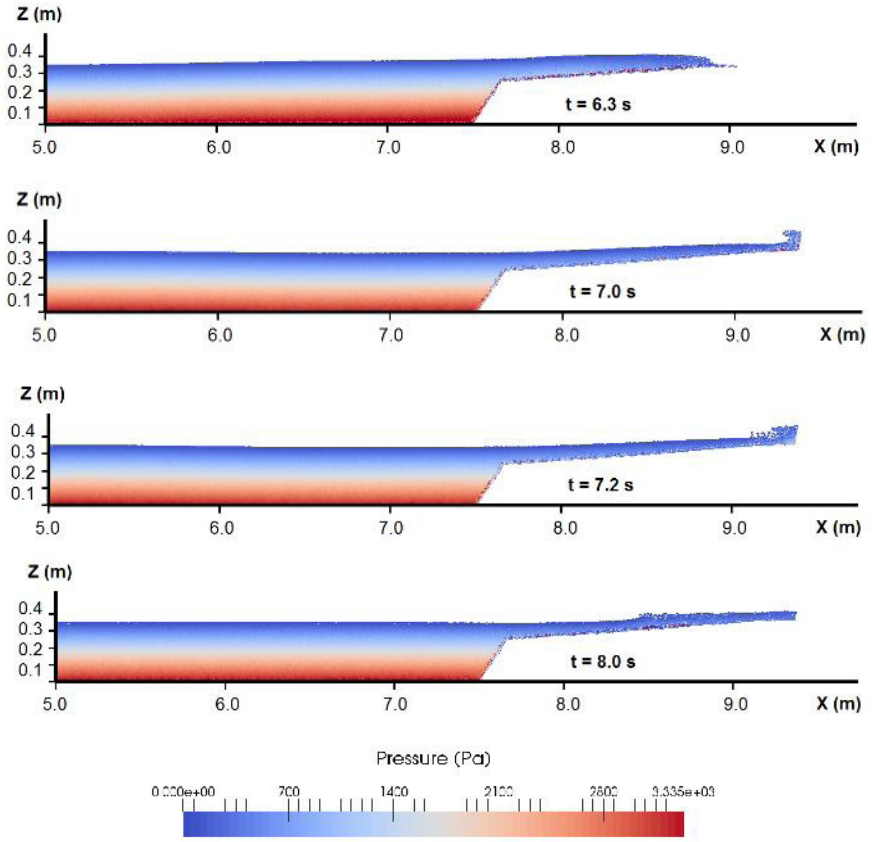

Fig. 4. Solitary wave profiles and pressure fields for $H_0 = 0.055$ m.

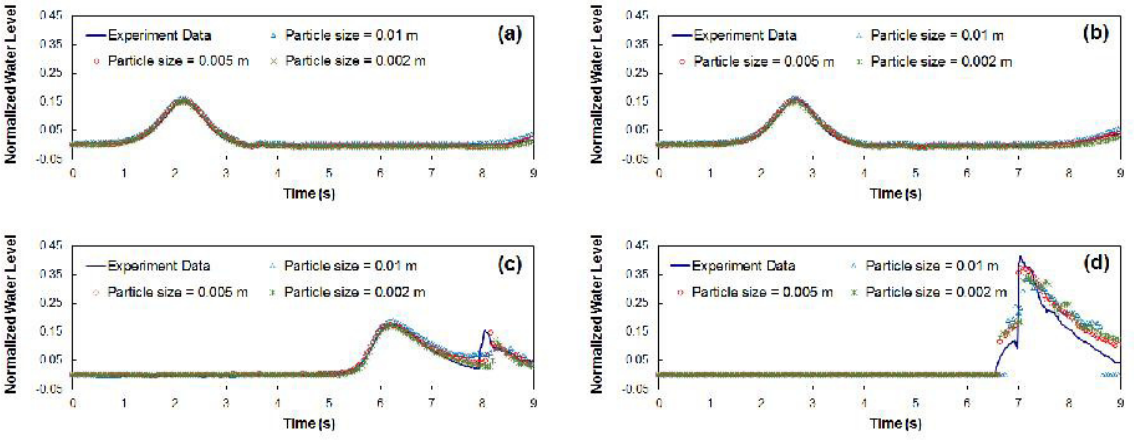

Fig. 5. Time history of water levels at the four monitoring points: (a) S1; (b) S2; (c) S3 and (d) S4 by the SPH model and experimental measurements for $H_0 = 0.055$ m. The normalized water levels are normalized by the mean water depth d.

Fig. 6 compares the SPH results at the location corresponding to the toe of the cliff under scenarios with and without the steep cliff. It is evident that the presence of the steep cliff introduces additional inundation at the location. Instead of a long and gradual propagation up and down the gentle slope, the wave front interacts with the cliff and water builds up rapidly at the toe of the cliff. The amplification factor is approximately 1.0 for the small incident wave and 1.6 for the larger wave. As the potential energy converts to kinematic energy, the accumulated water retreats away from the cliff. The slopes of the water level decrease in Fig.6 indicate that the steeper the incident wave, the faster the drawback process. The simulated normalized water level becomes less stable after it reaches approximately 0.1d due to limited particle supports as explained above. It corresponds to three to four particle spacing above the solid boundary at the location, which is at approximately 0.03d.

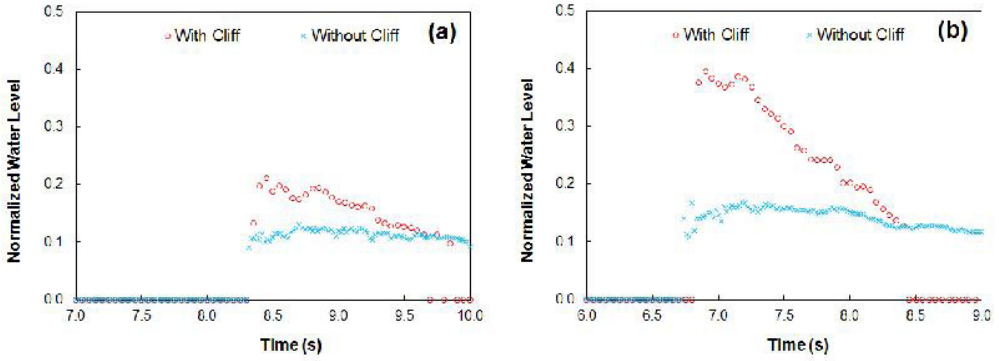

Fig. 6. Comparison of the water levels during the contact period at the toe of the cliff for H_0 = (a) 0.025 m and (b) 0.055 m with and without the presence of the steep cliff. The results are from simulations with particle size of 0.005 m. The normalized water level are normalized by the mean water depth d.

4. Conclusions

The evolution of solitary waves and the subsequent run-up on a steep onshore cliff has been investigated using the SPH-based DualSPHysics model. A complex onshore topography that consists of a steep offshore, a gentle onshore and a steep coastal cliff was used for the study. Tests for two incident wave were performed for both non-breaking and slight-breaking waves. In both cases, the SPH model was able to reproduce the wave profiles accurately along the wave flume for both offshore and onshore sections. The numerical results for time history of water levels at four gauges compared well with the laboratory measurements. The slight discrepancy in the drawback process rate observed in the small incident wave scenario was thought to be mainly caused by the lack of kernel support in the mild beach region where the slope is gentle and water depth is shallow. The performance of the SPH model was constrained by the number of particles available at shallow depths and the fluctuations in the pressure field near solid boundaries when the incident wave amplitude is small.

Acknowledgements

The authors acknowledge the support from the Singapore Maritime Institute Deepwater Technology (DWT) R&D Programme (SMI-2014-OF-10) and Earth Observatory of Singapore (EOS).

References

Crespo, A.J.C., Gómez-Gesteira, M., Dalrymple, R.A., 2007. Boundary conditions generated by dynamic particles in SPH methods. Computers, Materials and Continua 5(3), 173-184.

Crespo, A.J.C., Domínguez, J.M., Barreiro, A., Gómez-Gesteira, M., Rogers, B.D., 2011. GPUs, a new tool of acceleration in CFD: efficiency and reliability on Smoothed Particle Hydrodynamics methods. PLos ONE 6(6), e20685.

Dalrymple, R.A., Rogers, B.D., 2006. Numerical modelling of water waves with the SPH method. Coastal Engineering 53(2-3), 141-147.

Domínguez, J.M., Crespo, A.J.C., Gómez-Gesteira, M., Marongiu, J.C., 2011. Neighbouring lists in Smoothed Particle Hydrodynamics. International Journal of Numerical Methods in Fluids 67, 2026-2042.

Domínguez, J.M., Crespo, A.J.C., Gómez-Gesteira, M., 2013a. Optimization strategies for CPU and GPU implementations of a smoothed particle hydrodynamics method. Computer Physics Communications 184(3), 617-627.

Domínguez, J.M., Crespo, A.J.C., Valdez-Balderas, D., Rogers, B.D., Gómez-Gesteira, M., 2013b. New multi-GPU implementation for Smoothed Particle Hydrodynamics on heterogeneous clusters. Computer Physics Communications 184, 1848-1860.

Gingold, R.A., Monaghan, J.J., 1977. Smoothed particle hydrodynamics: Theory and application to non-spherical stars. Royal Astronomical Society, Monthly Notices 181, 375-389.

Gómez-Gesteira, M., Rogers, B.D., Dalrymple, R.A. and Crespo, A.J.C., 2010. State-of-art of classical SPH for free-surface flows. Journal of Hydraulic Research 48, 6-27.

Gómez-Gesteira, M., Crespo, A.J.C., Rogers, B.D., Dalrymple, R.A., Domínguez, J.M., 2012a. SPHysics - development of a free-surface fluid solver - Part 1: Theory and Formulations. Computers and Geosciences 48, 289-299.

Gómez-Gesteira, M., Rogers, B.D., Crespo, A.J.C., Dalrymple, R.A., Domínguez, J.M., Barreiro, A., 2012b. SPHysics - development of a free-surface fluid solver - Part 2: Efficiency and test cases. Computers and Geosciences 48, 300-307.

Hill E., Borrero, J.C.,Huang, Z.H., Qiu Q., Banerjee, P., Natawidjaja, D.H., Elosegui, P., Fritz, H.M., Suwargadi, B.W., Pranantyo, I.R., Li, L. L.,Macpherson, K.A., Skanavis, V., Synolakis C.E., Sieh, K., 2012. The 2010 Mw 7.8 Mentawai earthquake: Very shallow source of a rare tsunami earthquake determined from tsunami field survey and near-field GPS data. Journal of Geophysical Research 117 B06402, 21.

Huang, Z.H., Wu, T-R., Chen, T-Y., Sim, Y.S., 2013. A possible mechanism of destruction of coastal trees by tsunamis: A hydrodynamic study on effects of coastal steep hills. Journal of Hydro-Environment Research 7, 113-123.

Katell, G. and Eric, B., 2002. Accuracy of solitary wave generation by a piston wave maker. Journal of Hydraulic Research 40(3), 321-331.

Liu, M.B., Liu, G.R., 2010. Smoothed Particle Hydrodynamics (SPH): an Overview and Recent Developments. Archives of Computational Methods in Engineering 17(1), 25-76.

Lo, E.Y.M. and Shao, S.D., 2002. Simulation of near-shore solitary wave mechanics by an incompressible SPH method. Applied Ocean Research 24, 275-286.

Lucy, L., 1977. A numerical approach to the testing of fission hypothesis. The Astronomical Journal 82 (12), 1013–1024.

Monaghan, J.J., 1992. Smoothed Particle Hydrodynamics. Annual Review of Astronomy and Astrophysics 30, 543–574.

Monaghan, J.J., 1994. Simulating free surface flows with SPH. Journal of Computational Physics 110, 399-406.

Monaghan, J.J., Kos, A.M., 1999. Solitary waves on a Cretan beach. Journal of Waterway, Port, Coastal and Ocean Engineering 125(3), 145-154.

Rogers, B.D., Dalrymple, R.A., 2008. SPH Modeling of tsunami waves, Advances in Coastal and Ocean Engineering 10, Advanced Numerical Models for Tsunami Waves and Runup. World Scientific.

Shao, S.D., 2005. SPH simulation of solitary wave interaction with a curtain-type breakwater. Journal of Hydraulic Research 43(4), 366–375.

Wendland, H., 1995. Piecewise polynomial, positive definite and compactly supported radial functions of minimal degree. Advances in Computational Mathematics 4(1), 389-396.